Effects of water-emission anisotropy on multispectral remote sensing at thermal wavelengths of ocean temperature and of cirrus clouds

J. Otterman, J. Susskind, G. Dalu, D. Kratz, and I. L. Goldberg

The assumption of blackbody emission (emissivity, 1.0) for a calm ocean surface can lead to significant underestimates of the sea-surface temperature (SST) derived from IR radiometric data. Taking the optical properties of the atmosphere as known, we calculate the errors stemming from the blackbody assumption for cases of a purely absorbing or a purely scattering atmosphere. It is observed that for an absorbing atmosphere the errors in SST are always reduced and are the same whether measurements are made from space or at any level in the atmosphere. As for atmospheric scattering, the SST errors are slightly reduced when one is viewing from large zenith angles but are slightly enhanced when one is viewing from the zenith. The inferred optical thickness τ of an absorbing layer can be in error under the blackbody assumption by a $\Delta\tau$ of 0.01–0.08, while the inferred optical thickness of a scattering layer can be in error by a larger amount, $\Delta\tau$ of 0.03–0.13. The error $\Delta\tau$ depends only weakly on the actual optical thickness and on the viewing angle, but it is rather sensitive to the wavelength of the measurement. In the absence of steep slopes in the wave-slope distribution, directional emissivities are essentially unchanged by sea state when one is viewing from or near the zenith. When one is viewing from moderately large zenith angles (such as 50°), however, the departures in the directional emissivities from blackbody emission can be much larger under perturbed sea state than under calm conditions.

1. Introduction

In this study we examine the effects of the anisotropy of water emission on the remote sensing of two important climate-related parameters: the determination of sea-surface temperature (SST) and the long-wave characterization of cirrus clouds. Anisotropy means nonunity emissivity (lower than 1.0) and changing with the view direction.

Cirrus clouds, even though optically thin, are thought to have a significant influence on the climate, first by a reduction of the intake of the solar radiation by the surface-atmosphere system and second by a blanketing effect in the thermal infrared, i.e., a partial replacement of the high-temperature emission to space from the surface (and near surface) by their own emission to space at their low temperature. Because the short-wave effect of cirrus clouds induces a cooling, whereas the long-wave effect alone induces a warming, it is important to assess each effect accurately to appropriately evaluate the net effect. The long-wave blanketing effect depends on the optical thickness of the cloud layer, its scattering versus absorbing characteristics, and its temperature. These parameters have been derived by remote sensing in the spectral window regions from nadir-viewing instruments.[1,2]

Satellites, with their synoptic coverage, can serve as a highly important source of SST data, providing a global supplement to the more accurate but spatially inadequate ship reports.[3–8] High accuracy is required for these measurements to be useful as climatic data sets. For instance, the increase by 0.1°C in global SST over a 6.5-yr period reported by Strong[8] from satellite observations has been challenged as probably spurious by Reynolds *et al.*,[9] who did not observe such a change in the *in situ* measurements.

J. Otterman's permanent address is Tel Aviv University, Ramat Aviv, Israel; his current address is NASA/Goddard Space Flight Center, Code 911, Greenbelt, Maryland 20771; J. Susskind and I. L. Goldberg are with NASA/Goddard Space Flight Center, Greenbelt, Maryland 20771; G. Dalu is with the Consiglio Nazionale delle Ricerche, Istituto di Fisica dell' Atmosfera, Rome, Italy; D. Kratz is with Universities Space Research Associates, NASA/Goddard Space Flight Center, Greenbelt, Maryland 20771.

Received 26 July 1992.
0003-6935/92/367633-14$05.00/0.

The advanced very high resolution radiometer (AVHRR) on the National Oceanographic and Atmospheric Administration satellites supply the SST in cloud-free areas with an accuracy of 0.7 K in midlatitudes and a somewhat poorer accuracy in tropical regions, where water vapor absorbs much of the surface-emitted infrared radiation. The current requirement for global numerical climate models is specified as 0.3 K.[10] Temperature mapping with an accuracy lower than that required for a climate record can play a useful role in observing climate-affecting SST anomalies.[6,11]

In SST retrieval and in the long-wave characterization of cirrus clouds from multispectral measurements, radiative transfer through the atmosphere is calculated with high accuracy.[12] The emission from the ocean surface, however, is often considered simply as that of a blackbody. This is a questionable assumption, because the emissivity at the nadir (where the emissivity is largest) is by 1 to 5 percent lower than unity (depending on the wavelength) and drops to low fractions at the large-view zenith angles.[13–16] The zenith-angle dependence has been ignored in the inversion of satellite measurements even in the studies where the nonblackbody emissivity of water has been addressed, such as in Susskind and Reuter.[7] For a calm ocean this low emissivity (high reflectance) near the horizon is so pronounced that in these directions it is the emission of the atmosphere reflected from the water that is predominantly observed, rather than the emission from the water. Radiation temperatures measured at near-glancing angles may provide information about the effective emissivity, and therefore about the sea state.[17] As a source of information about SST, measurements at these directions are essentially useless. We mention these effects because they are somewhat relevant to sea-state effects on measurements at a 50° zenith angle, which we discuss in Appendix A.

The nature of the problem is discussed in Section 2. In Section 3, a parameterization of calm-water spectral emittances and reflectances is presented in a formulation appropriate for atmospheric radiative transfer calculations. The consequences of nonblackbody emission are then assessed for the retrieval of the SST and for the long-wave characterization of optically thin clouds. The errors are computed in the SST retrieved under the blackbody assumption without an atmosphere, either below or above the measuring radiometer, and also under a scattering or absorbing atmosphere. Two cases of an absorbing atmosphere are analyzed. In the case of absorption by a high cirrus cloud the assigned temperature is 70 K lower than that of the surface, whereas in the case of absorption by water vapor in the mixed layer the temperature is equal to that of the surface.

At the long-wave wavelengths that we discuss, atmospheric absorption strongly predominates over scattering. In the case of cirrus clouds, however, scattering is certainly significant. The single-scattering albedo of large spherical ice particles and water drops can exceed 0.8 in a range of wavelengths (see Table 1 in Ref. 2). For these large particles the phase function has a strong forward peak, for which propagation without extinction can be assumed. For small particles the single-scattering albedo is much smaller, but the phase function is less anisotropic. We analyze scattering effects separately from the absorption effects. In the analysis of the SST retrieval, i.e., in inverting our expressions for the radiometer reading, perfect specification of the atmosphere is assumed. The effects of imperfect information about the atmosphere, especially about the water-vapor absorption, deserve a separate study.

2. Nature of the Problem in Sea-Surface-Temperature Retrieval and Cirrus Cloud Characterization

Two related problems of SST retrieval are discussed here. Assuming that the signal $B(T_m)$, where B denotes the spectral Planck function and T_m is the measured temperature, is measured perfectly (a noiseless radiometer), what are the errors in (a) the inferred SST and (b) the optical thickness of the atmosphere, caused by the assumption of blackbody water emission? In discussing question (a) we assume that the information about the atmospheric profile is perfect, whereas concerning question (b) we assume that the water temperature T_s is known exactly. Question (a) has been analyzed by Dalu[18] for zenith viewing in the 11-μm split-window bands of the AVHRR based on the emissivity and reflectance model for these bands by Takashima and Takayama.[19] Our examination is in a broad range of wavelengths, viewing from the zenith and from the zenith angle of 50°.

In this section simplified equations are presented that sketch out how the radiation temperature reading by a satelliteborne or aircraftborne radiometer depends on the water temperature, its emissivity, and the atmospheric properties. [These equations are not used in the numerical analysis later; we discuss remote sensing of the ocean temperature by applying Eqs. (16) and (18) in the case of absorbing atmosphere and Eqs. (25) and (26) in the case of scattering atmosphere.] The radiometer spectral signal is represented by the atmosphere-surface system directional (monochromatic) emittance $B(T_m)$ ($\mathrm{Wm^{-2}\ \mu^{-1}}$), where T_m is the radiation temperature measured at a given zenith angle and B is the spectral Planck function for the wavelength of measurement. (The equivalent concept in short-wave modeling, i.e., in modeling reflectances at the solar wavelengths, is the product of the directional spectral illumination and the bidirectional reflectance factor). The monochromatic radiance ($\mathrm{Wm^{-2}\ \mu m^{-1}\ sr^{-1}}$), defined as the signal measured from a unit horizontal target when the temperature is absolute zero outside the target area, is $\cos\theta\, B(T_m)/\pi$, where θ is the viewing zenith angle. Integration of the radiances over a hemisphere (radiance multiplied by the differential solid angle 2π

$\sin\theta\, d\theta$) produces the monochromatic flux ($Wm^{-2}\ \mu m^{-1}$), which in our convention is represented by the spectral Planck function $B(\overline{T}_m)$, where $\overline{T}_m$ is the effective temperature measured over the hemisphere.

The spectral Planck function of the water temperature T_s is $B(T_s)$, and $U(\tau_a)$ and $D(\tau_a)$ are the spectral Planck functions of directional emittance from the atmosphere in the upward and downward directions respectively (at the zenith angle θ), as modified by scattering within the atmosphere but excluding any contribution from the surface emission, whether transmitted through or scattered by the atmosphere. These two Planck functions depend on the absorbing (emitting) atmospheric optical thickness τ_a, the temperature and the vertical profile of the absorbers (emitters), and on the zenith angle of viewing θ. We explicitly indicate the dependence on τ_a to stress that $U(\tau_a)$ and $D(\tau_a)$ describe the emission from the atmosphere.

Distinct components can be identified in $B(T_m)$ when viewing from within or above an atmosphere. Some of the components are amplified by backscattering from below the atmosphere and surface reflection. Only one backscattering from the atmosphere, followed by a reflection from the surface, is considered. The six components are as follows.

The first component is the fraction of the surface signal $\epsilon(\theta)B(T_s)$ that penetrates directly through the atmosphere (whether scattering or absorbing), where $\epsilon(\theta)$ is the directional emissivity. When $t(\theta)$ designates the directional transmittance through the atmosphere, this componant is $\epsilon(\theta)B(T_s)t(\theta)$.

The second component is the downward directional emission from the atmosphere $D(\tau_a)$ (as modified by scattering within the atmosphere, if any) at zenith angle θ, which is first reflected in mirrorlike reflection from the water with directional reflectance $1 - \epsilon(\theta)$ and then penetrates through the atmosphere. This component is amplified by backscattering from the atmosphere and water reflection; considering atmospheric backscattering [with coefficient $b(\theta)$ from a direction up to the same direction down] and a surface reflection, we find that this component is $D(\tau_a)[1 - \epsilon(\theta)]t(\theta)\{1 + [1 - \epsilon(\theta)]b(\theta)\}$.

The third component is the downward flux emitted from the atmosphere $F_d(\tau_a)$ (as modified by scattering within the atmosphere, if any) that is reflected from the water with the hemispheric reflectance $1 - \epsilon_h$ (where ϵ_h is the hemispheric emissivity) and is then scattered upward to the satellite, with scattering coefficient $\bar{f}(\theta)$. Backscattering from the atmosphere (with backscattering coefficient $\overline{b}_h$ from hemisphere up to hemisphere down) and subsequent reflection from the water amplify this component by a factor $[1 + (1 - \epsilon_h)\overline{b}_h]$, and thus this component is $F_d(\tau_a)(1 - \epsilon_h)\bar{f}(\theta)[1 + (1 - \epsilon_h)\overline{b}_h]$.

The fourth component is the scattering upward by the atmosphere of the surface-emitted flux $\epsilon_h B(T_s)$, where ϵ_h is the hemispheric emissivity; if $\bar{f}(\theta)$ is the directional scattering coefficient for the flux $\epsilon_h B(T_s)$, this term is $\epsilon_h B(T_s)\bar{f}(\theta)$. Note that the value of $\bar{f}(\theta)$ depends on θ, the zenith angle at which the observed radiance emerges from the top of the atmosphere; $\bar{f}(\theta)$ also depends on the distribution of the directional surface emissivity with the zenith angle [i.e., $\epsilon_h \bar{f}$ is the integral in the zenith angle θ of $\cos\theta \sin\theta\, \epsilon(\theta)f(\theta)$]. Backscattering from the atmosphere with backscattering coefficient $\overline{b}_h$ (from hemisphere up to hemisphere down) and a surface reflection amplify this component; it is thus $\epsilon_h B(T_s)\bar{f}(\theta)[1 + (1 - \epsilon_h)\overline{b}_h]$.

The fifth component is the backscattering from the atmosphere to a specific direction [with coefficient $b_h(\theta)$ from the hemisphere up to one direction down] of the surface-emitted flux, which after reflection from water with reflectance $1 - \epsilon(\theta)$ penetrates through the atmosphere. Without considering second and higher backscattering from the atmosphere and surface reflection, we find that this component is $\epsilon_h B(T_s)b_h(\theta)[1 - \epsilon(\theta)]t(\theta)$.

The sixth component is the upward directional emission at zenith angle θ solely by the atmosphere, $U(\tau_a)$; for water temperature T_s at absolute zero, we would have $U(\tau_a) = B(T_m)$.

The errors in retrieved temperatures are now discussed in general terms; $B(T_m)$ is differentiated with respect to $B(T_s)$ and the surface emissivity, or rather the emissivities, $\epsilon(\theta)$ and ϵ_h. From the first, fourth, and fifth components we obtain

$$\frac{dB(T_m)}{dB(T_s)} = t[\epsilon + \epsilon_h(1 - \epsilon)b_h] + \epsilon_h\bar{f}[1 + (1 - \epsilon_h)\overline{b}_h]; \tag{1}$$

from the first, second, and fifth components we obtain

$$\frac{dB(T_m)}{d\epsilon} = B(T_s)t(1 - \epsilon_h b_h) - D(\tau_a)t[1 + 2(1 - \epsilon)b]; \tag{2}$$

and from the third, fourth, and fifth components we obtain

$$\frac{dB(T_m)}{d\epsilon_h} = B(T_s)\{\bar{f}[1 + (1 - 2\epsilon_h)\overline{b}_h] + (1 - \epsilon)tb_h\} - F_d(\tau_a)\bar{f}[1 + 2(1 - \epsilon_h)\overline{b}_h], \tag{3}$$

where we omit θ from ϵ, t, $\bar{f}$, b, and b_h.

The error $\Delta B(T_s)$ in $B(T_s)$ resulting from the emissivity errors, $\Delta\epsilon$ in ϵ and $\Delta\epsilon_h$ in ϵ_h, is specified by this generally applicable relation:

$$\Delta B(T_s)\frac{dB(T_m)}{dB(T_s)} = -\Delta\epsilon\frac{dB(T_m)}{d\epsilon} - \Delta\epsilon_h\frac{dB(T_m)}{d\epsilon_h}. \tag{4}$$

Under the blackbody assumption the errors in the emissivity are $\Delta\epsilon = 1 - \epsilon$ and $\Delta\epsilon_h = 1 - \epsilon_h$. Thus,

specifying the derivatives from Eqs. (1) and (2), we see that Eq. (4) becomes

$$\Delta B(T_s)\{t[\epsilon + \epsilon_h(1-\epsilon)b_h] + \epsilon_h \bar{f}[1 + (1-\epsilon_h)\bar{b}_h]\}$$
$$= -(1-\epsilon)t\{B(T_s)(1-\epsilon_h b_h) - D(\tau_a)[1 + 2(1-\epsilon)b]\}$$
$$-(1-\epsilon_h)\{\bar{f}B(T_s)[1 + (1-2\epsilon_h)\bar{b}_h]$$
$$+ tB(T_s)(1-\epsilon)b_h - \bar{f}F_d(\tau_a)[1 + 2(1-\epsilon_h)\bar{b}_h]\}. \quad (5)$$

Good insight into the problem can be gained most easily by separately considering a case of a purely absorbing atmosphere and a case of a purely scattering atmosphere (we adopt the same approach in the numerical discussion in later sections). In the absorbing-atmosphere case, Eq. (5) applies with $\bar{f} = b_h = \bar{b}_h = b = 0$. The error, denoted by Δ_a, is

$$\Delta_a B(T_s) = -(1-\epsilon)\frac{B(T_s) - D(\tau_a)}{\epsilon}, \quad (6)$$

where the directional transmittance t has canceled out and thus does not influence the error. This conclusion would be quite inappropriate in the case of a noisy, i.e., real radiometer, inasmuch as the surface-signal component $\epsilon t B(T_s)$ is proportional to t; a smaller t means a reduced signal-to-noise ratio. The error is proportional to $(1-\epsilon)/\epsilon$, and the hemispheric reflectance $1-\epsilon_h$ plays no role. Furthermore, it is observed that with a larger downward atmospheric emission $D(\tau_a)$ the underestimate $\Delta_a B(T_s)$ becomes smaller. $D(\tau_a)$ increases for a larger atmospheric optical thickness τ_a and a higher atmospheric temperature. Because t canceled out, Eq. (6) applies to satellite measurements as well to aircraft measurements at any level *within* the atmosphere. This application will include low-level flights for which $t \approx 1.0$.

In the pure scattering case we have $D(\tau_a) = F_d(\tau_a) = U(\tau_a) = 0.0$. The error, denoted by Δ_s, is

$$\frac{\Delta_s B(T_s)}{B(T_s)} = -\frac{(1-\epsilon)t[1 + (1-2\epsilon_h)b_h] + (1-\epsilon_h)\bar{f}[1 + (1-2\epsilon_h)\bar{b}_h]}{t[\epsilon + \epsilon_h(1-\epsilon)b_h] + \epsilon_h\bar{f}[1 + (1-\epsilon_h)\bar{b}_h]}. \quad (7)$$

It should be noted that both t and $\bar{f}$ are retained in the expression for the error, and that the hemispheric reflectance $1-\epsilon_h$ appears alongside the directional reflectance $1-\epsilon$. With increasing optical thickness between the surface and the radiometer, t decreases while $\bar{f}$ can increase, and thus the errors in the measurements within the atmosphere generally will be quite different than in the measurements from space, and these errors will depend on the altitude of the aircraft.

In Eqs. (6) and (7) above, retrieval errors under a purely absorbing or a purely scattering atmosphere are respectively formulated. The scattering–absorption cross products are thus omitted from the discussion. These terms carry a positive sign, i.e., the scattering–absorption cross effects tend to reduce the underestimate of the water temperature.

3. Characterization of Calm-Water Emission

Information about water emissivity has been surveyed and collected by Sidran.[15] A useful tabulation of water spectral reflectances is given by Bramson[14] for nine zenith angles (from $\theta = 0°$ to $\theta = 80°$) in the spectral range from 9.2 to 15 μm. The directional reflectance $1-\epsilon(\theta)$ for $\theta = 0°$ and $\theta = 50°$ from Bramson's Table 196 is presented in Fig. 1A. We note that the reflectance at 50° is nearly twice that at 0°, and that from 11 μm to 15 μm there is an increase in the reflectance with the wavelength by a factor of 5.

In computing the radiances measured from the satellite for the case of a scattering layer (i.e., when single-scattering albedo ω_0 is not zero), we find that the hemispheric reflectance $1-\epsilon_h$ is involved in addition to the directional reflectance $1-\epsilon(\theta)$. The hemispheric reflectance is

$$1 - \epsilon_h = 1 - 2\pi\int_0^{\pi/2} \cos\theta \sin\theta\epsilon(\theta)d\theta/\pi$$
$$= 1 - 2\int_0^1 \mu\epsilon(\mu)d\mu, \quad (8)$$

where $\mu = \cos\theta$.

Alongside the two directional reflectances, in Fig. 1A we plot the hemispheric reflectance $1-\epsilon_h$ computed from Bramson's tabulation. The hemispheric emissivity ϵ_h is computed by the formula

$$\epsilon_h = \left(\sum_{10°}^{80°} \cos\theta \sin\theta\right)^{-1} \sum_{10°}^{80°} \cos\theta \sin\theta\epsilon(\theta), \quad (9)$$

where $\epsilon(\theta)$ takes Bramson's[14] values for the eight zenith angles from 10° to 80°.

For our atmospheric radiative transfer calculations, we find it appropriate to represent the directional emissivity as a function of the zenith angle by a simple exponential expression:

$$\epsilon_a(\mu) = c\exp(-m/\mu). \quad (10)$$

The coefficients c and m, obtained by fitting the directional emissivity ϵ_a to Bramson's data at $\theta = 0°$

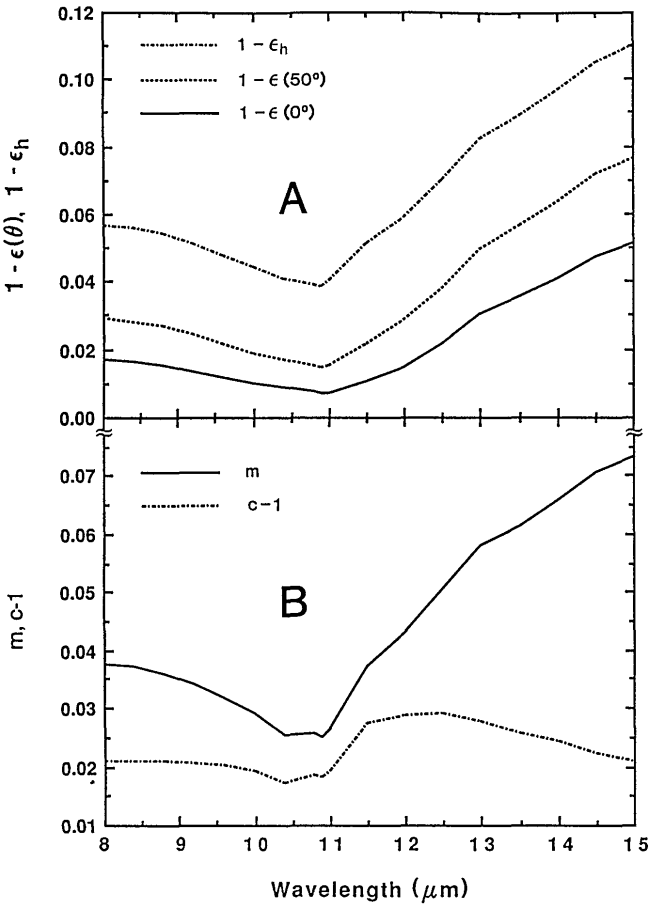

Fig. 1. A Spectral reflectances versus wavelength, directional reflectances $1 - \epsilon(0°)$ and $1 - \epsilon(50°)$ from Bramson's tabulation,[14] and hemispheric reflectance $1 - \epsilon_h$ fitted to Bramson's data. B Coefficients $c - 1$ and m in the approximate representation of the spectral directional emissivity.

and to the hemispheric emissivity ϵ_h, as computed by Eq. (9) are plotted versus wavelength in Fig. 1B.

4. Sea-Surface-Temperature Retrieval Without Atmosphere

Assuming no atmospheric emission, absorption, or scattering, we find that the temperature $T_m(\theta)$ remotely measured at a zenith angle θ is

$$T_m(\theta) = B^{-1}[\epsilon(\theta)B(T_s)], \tag{11}$$

where B^{-1} denotes the inverse of the Planck Function for the wavelength of the measurement and T_s is the water temperature. If $\epsilon(\theta) = 1.0$, $T_m(\theta) = T_s$. In the case of an anisotropic surface emission, the blackbody assumption (under which T_s is equated to T_m) leads to an error ΔT_s in the SST retrieval given by the expression

$$\Delta T_s = T_m(\theta) - T_s = B^{-1}[\epsilon(\theta)B(T_s)] - T_s. \tag{12}$$

The error ΔT_s, which is obviously always negative because $\epsilon(\theta)$ is always less than 1.0, is plotted for two viewing directions, $\theta = 0°$ in Fig. 2A and $\theta = 50°$ in Fig. 3A, for surface temperature $T_s = 300$ K in each case.

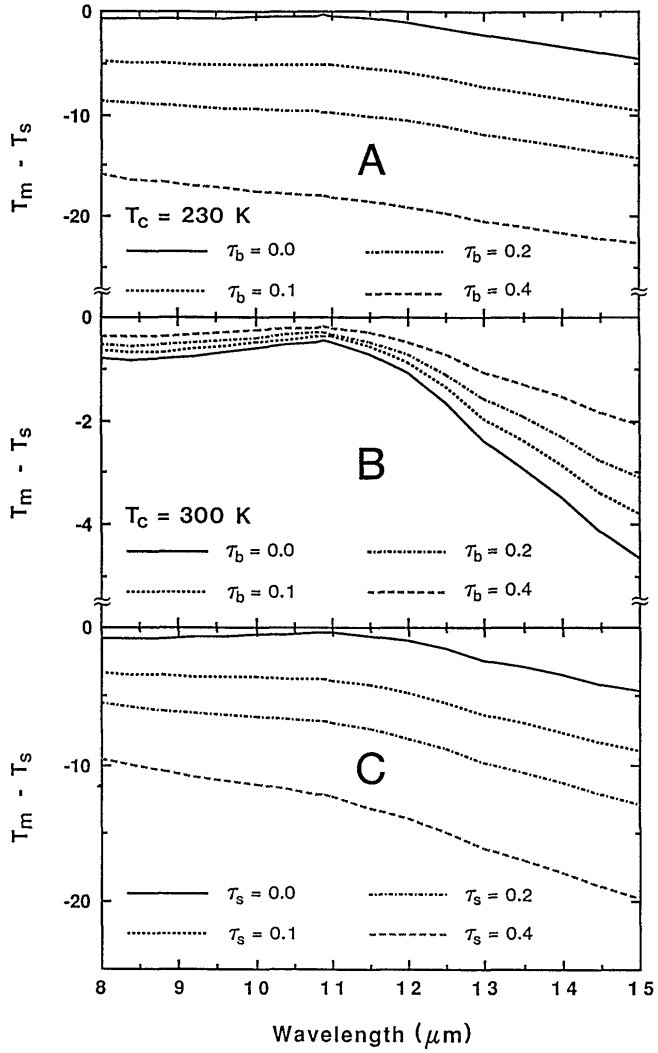

Fig. 2. Temperature differences versus wavelength $T_m - T_s$, when T_m is measured from the zenith: A without an atmosphere and over an absorbing layer τ_b, $T_c = 230$ K; B as in Fig. 2A, but T_c is equal to SST, $T_c = 300$ K; C over a scattering layer τ_s.

The error in the SST retrieval can be assessed with satisfactory accuracy by a much simpler expression, as discussed by Kornfield and Susskind.[20] In the 8- to 15-μm region, the Planck function for the emission from the ocean with the temperature T_s of ~300 K can be approximated by Wien's law, $c_1\lambda^{-5}\exp(-c_2/\lambda T_s)$, where c_1 is the first radiation constant, c_2 is the second radiation constant, and λ is the wavelength of the measurement (see, e.g., Ref. 21). If the Planck function of the measured temperature $B(T_m)$ is given as $\epsilon c_1\lambda^{-5}\exp(-c_2/\lambda T_s)$, the errors $\Delta\epsilon$ in the directional emissivity and ΔT_s in the inferred temperature are related by the equation $\Delta T_s[dB(T_m)/dT_s] = -\Delta\epsilon[dB(T_m)/d\epsilon]$. From this differentiation we obtain

$$\Delta T_s = -(1 - \epsilon)\epsilon^{-1}\lambda T_s^2 c_2^{-1}, \tag{13}$$

where $c_2 = 14{,}388$ μm K, because the blackbody assumption constitutes an emissivity error of $1 - \epsilon$.

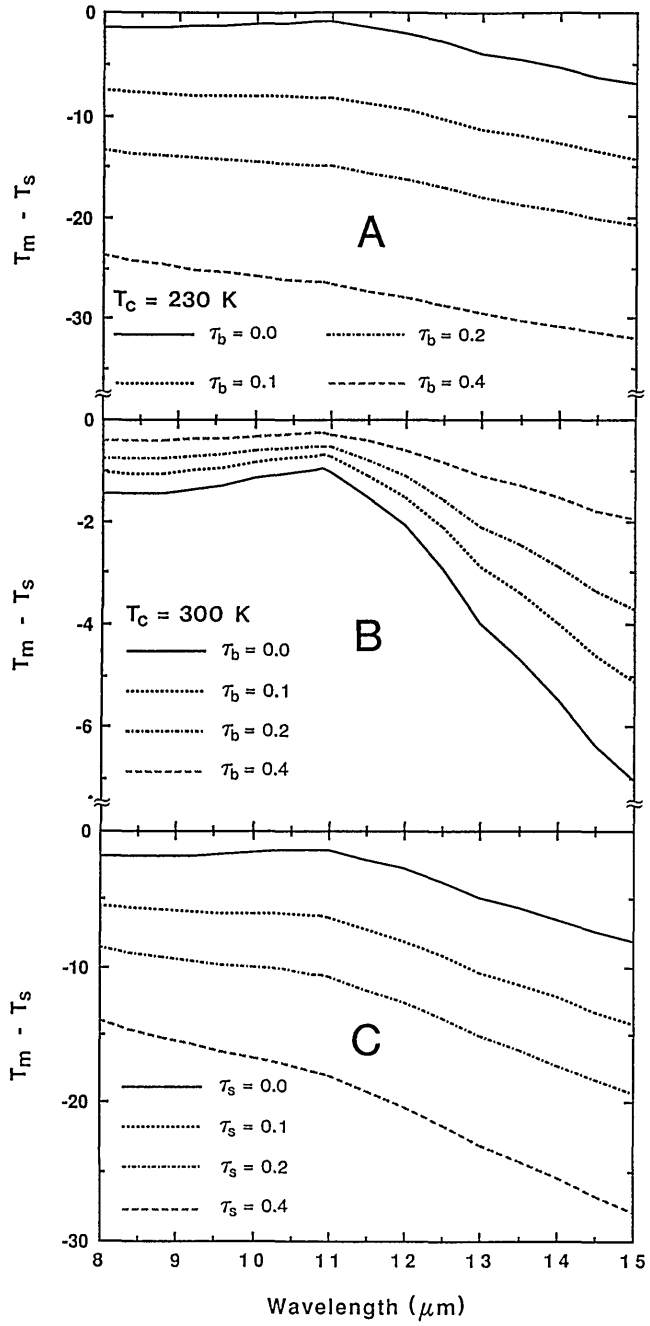

Fig. 3. Temperature differences $T_m - T_s$ as in Fig. 2 but with T_m measured at $\theta = 50°$.

This relation gives the impression that the error linearly depends on the wavelength λ. Actually, the error primarily depends on the emissivity, which changes sharply with the wavelength. The dependence on the surface temperature T_s is not significant inasmuch as water temperatures would generally be in a narrow range.

5. Inferring Sea-Surface Temperature and Optical Thickness of an Atmospheric Layer in the Case of Atmospheric Absorption

In the case of atmospheric absorption, we consider the radiation temperature T_m [the cosine μ of zenith angle θ is omitted from $T_m(\mu)$ for the sake of simplicity] measured above a purely absorbing layer, characterized by a vertical optical thickness τ_b and a temperature T_c. The ocean surface temperature is T_s and its emission anisotropy is as tabulated by Bramson.[14] The temperature measurements can be most conveniently expressed by the Planck function $B(T_m)$ of the radiation temperature T_m observed above the layer. A measurement at a zenith angle θ involves three components: (a) the emission from the surface that penetrates through the layer, $\epsilon(\theta)B(T_s)\exp(-\tau_b/\mu)$, (b) the emission from the absorbing layer $B(T_c)[1 - \exp(-\tau_b/\mu)]$, and (c) the component $[1 - \epsilon(\mu)]B(T_c)[1 - \exp(-\tau_b/\mu)]\exp(-\tau_b/\mu)$ caused by downward emission from the layer, reflection from the surface, and transmission through the layer, where $\epsilon(\mu)$ is the directional emissivity. We assume a mirror reflection at the water surface, with reflectance $1 - \epsilon(\mu)$. We have

$$B(T_m) = \epsilon(\mu)B(T_s)\exp(-\tau_b/\mu) + B(T_c)[1 - \exp(-\tau_b/\mu)] \times \{1 + [1 - \epsilon(\mu)]\exp(-\tau_b/\mu)\}. \quad (14)$$

We compute the temperatures T_m by assuming T_s = 300 K. The temperature differences $T_m - T_s$ observed from the zenith, $\theta = 0°$, are presented for two atmospheric temperatures, T_c = 230 K and T_c = 300 K (i.e., equal to the water temperature) in Figs. 2A and 2B, respectively, for four values of τ_b (0.0, 0.1, 0.2, and 0.4). The corresponding $T_m - T_s$ temperature differences observed at $\theta = 50°$ are presented in Figs. 3A and 3B. The emissivity $\epsilon(\mu)$ in these two directions is specified in our calculations as given by Bramson (plotted versus wavelength in Fig. 1A). In the case T_c = 230 K, the observed temperatures T_m are much lower (by as much as 24 K) than the surface temperature T_s. In this case the $T_m - T_s$ differences increase (in the absolute value) with increasing optical thickness τ_b. In the case T_c = 300 K, which pertains to water-vapor absorption in the low mixed layer, these $T_m - T_s$ differences are much smaller (by a factor of ~ 5) and decrease with increasing τ_b. As we can anticipate from the emissivity data presented in Fig. 1A, the $T_m - T_s$ differences show a significant variation with the wavelength. The differences are larger when T_m is observed at $\theta = 50°$. The differentiation of $B(T_m)$ given by Eq. (14) with respect to τ_b establishes for what $B(T_c)/B(T_s)$ ratios T_m increases (i.e., the $T_m - T_s$ difference decreases in magnitude) with increasing optical thickness τ_b. The inequality

$$B(T_c)\left[1 + \frac{2(1 - \epsilon)}{\epsilon}\exp(-\tau_b/\mu)\right] > B(T_s) \quad (15)$$

spells out this condition, which applies to any view direction.

Inverting Eq. (14), we obtain an expression for the water temperature T_{sia} inferred from the measured

temperature T_m:

$$T_{\text{sia}} = B^{-1}\left[\frac{\exp(\tau_b/\mu)}{\epsilon(\mu)}(B(T_m) - \{1 + [1 - \epsilon(\mu)]\exp(-\tau_b/\mu)\} \times B(T_c)[1 - \exp(-\tau_b/\mu)])\right], \quad (16)$$

where T_{sia} stands for the inferred temperature accounting for the nonunity emission.

Under the assumption of a blackbody surface emission, there is no component caused by downward emission from the layer, reflection from the surface, and transmission through the layer. The measured temperature T_m is expressed by an equation simpler than Eq. (14):

$$B(T_m) = B(T_{\text{sbb}})\exp(-\tau_b/\mu) + B(T_c)[1 - \exp(-\tau_b/\mu)], \quad (17)$$

where the water temperature is denoted as T_{sbb}. Inversion of this equation for T_{sbb} yields

$$T_{\text{sbb}} = B^{-1}\{\exp(\tau_b/\mu)[B(T_m) - B(T_c)] \times [1 - \exp(-\tau_b/\mu)]\}. \quad (18)$$

With the atmosphere accurately specified, i.e., with the optical thickness τ_b and cloud temperature T_c known exactly, the measured T_m when applying Eq. (16) provides exact information about the water temperature, $T_{\text{sia}} = T_s$. Under the blackbody assumption the water temperature retrieval will be computed by Eq. (18) and thus will be in error by $\Delta T = T_{\text{sbb}} - T_s$ [T_m in Eq. (18) is specified by the value of T_s in Eq. (14)]. For $\theta = 0$ this difference is plotted for four values of optical thickness τ_b in Figs. 4A and 4B, for temperatures T_c of 230 and 300 K, respectively. We note a reduction in the errors compared with the no-atmosphere case, $\tau_b = 0$. The error reduction is hardly significant in the cirrus cloud case, $T_c = 230$ K, but the reduction is by a factor of $\sim 1/3$ (if $\tau_b = 0.4$) in the mixed-layer water-vapor case, $T_c = 300$ K. The error always becomes smaller for a larger optical thickness. The same pattern appears for viewing at $\theta = 50°$, shown in Figs. 5A and 5B for $T_c = 230$ K and $T_c = 300$ K, respectively, but the errors are much larger than at $\theta = 0°$.

If Eq. (17) is assumed to be valid and is applied to the inference of the vertical optical thickness of the layer based on the exact information concerning the water temperature T_s, this inferred optical thickness τ_{inf} is given by the logarithmic expression

$$\tau_{\text{inf}} = \mu \ln \frac{B(T_s) - B(T_c)}{B(T_m) - B(T_c)}. \quad (19)$$

The differences $\Delta\tau_b = \tau_{\text{inf}} - \tau_b$, i.e., the errors in inferring τ_b under the blackbody assumption, are plotted for the cirrus cloud case, $T_c = 230$ K, in Fig. 6A for viewing from the zenith and in Fig. 7A for viewing at zenith angle $\theta = 50°$. Note that $\Delta\tau_b$ is approximately the same for all four values of τ_b: $\Delta\tau_b$ is smallest, approximately 0.01, at 11 μm and increases to a range of 0.06–0.08 above 14 μm. The error $\Delta\tau_b$ is approximately the same (only slightly larger) at $\theta = 50°$ (Fig. 7A) as at $\theta = 0°$ (Fig. 6A). The error $\Delta\tau_b$ increases steeply from 11 to 14 μm, by ~ 0.05. This may be a significant difference when the variation with wavelength of the inferred optical thickness is used to assess the cloud particle-size distribution. For a mixed-layer water-vapor case, $T_c = T_s$, T_{inf} diverges according to Eq. (19), suggesting that the optical thickness of a near-surface layer is essentially indeterminate. The implication is that inferring the amounts of near-surface water vapor is impossible without appropriate information concerning the emissivity of the surface. The availability of this information does not necessarily mean that a satisfactory determination of water vapor is feasible, because of the many uncertainties involved in the inversion.

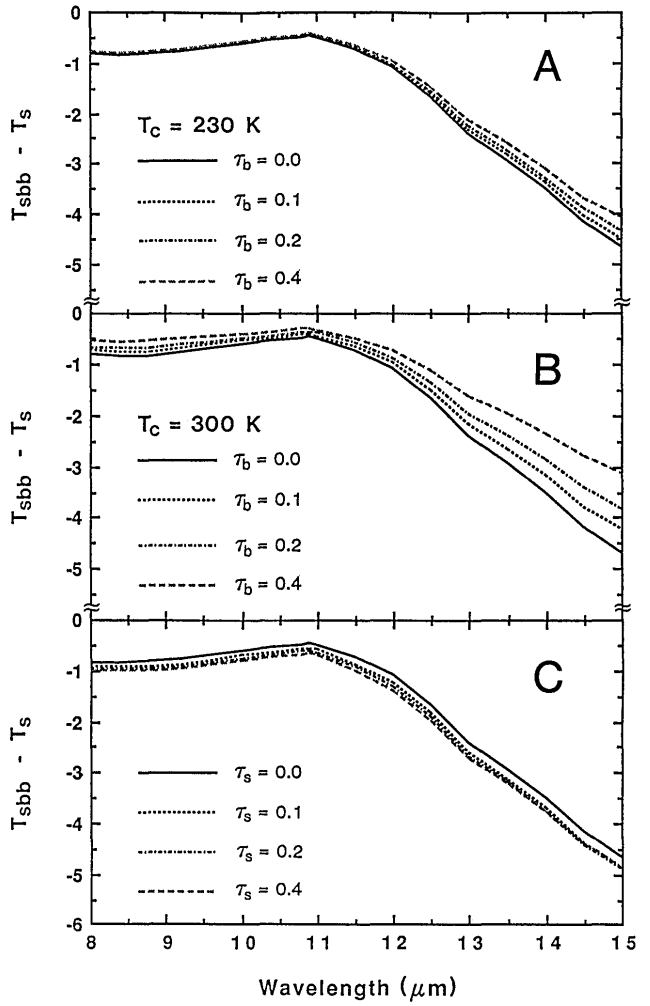

Fig. 4. Errors $\Delta T_s = T_{\text{sbb}} - T_s$ in the SST retrieval under the blackbody assumption viewing from the zenith: A without an atmosphere and over an absorbing layer τ_b, $T_c = 230$ K; B as in Fig. 4A but with T_c equal to the water temperature, $T_c = 300$ K; C over a scattering layer τ_s.

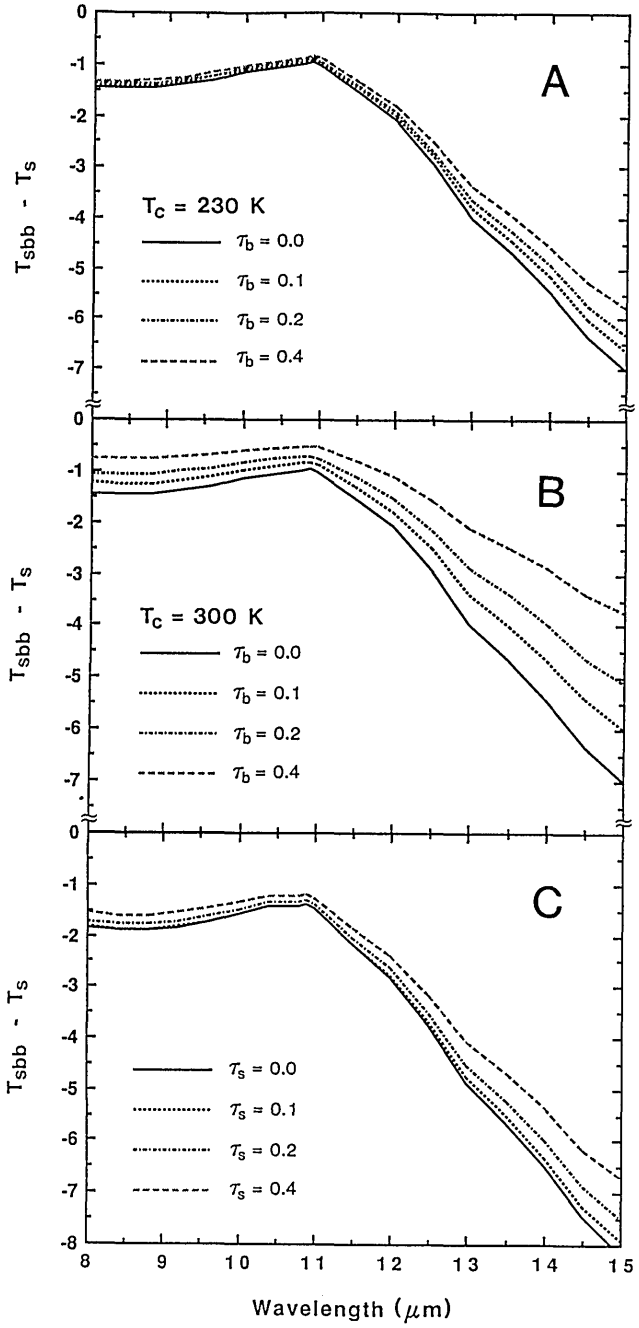

Fig. 5. Errors $\Delta T_s = T_{sbb} - T_s$ in the SST retrieval as in Fig. 4 but for viewing from $\theta = 50°$.

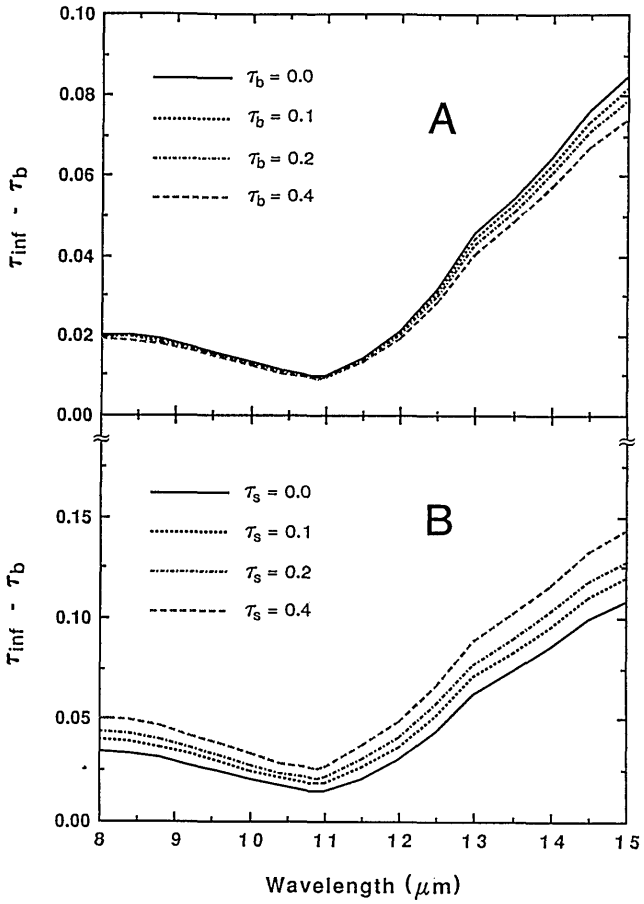

Fig. 6. Error in the inferred optical thickness under the blackbody assumption, viewing from the zenith: A error $\Delta\tau_b$ in the cirrus cloud-absorbing optical thickness, $T_c = 230$ K; B error $\Delta\tau_s$ in the scattering optical thickness.

6. Inferring Sea-Surface Temperature and Optical Thickness of an Atmospheric Layer in the Case of Atmospheric Scattering

We now consider measurements when the water surface is overlaid by a scattering layer. In contrast to Section 5, here water emissivities at all zenith angles influence the measurement at a single zenith angle θ. The directional emissivity $\epsilon(\theta)$ of the surface is specified here by a simple exponential in μ, Eq. (10), $\epsilon(\theta) \approx \epsilon_a(\theta) = c \exp(-m/\mu)$. Our approximation, which greatly simplifies the radiative transfer through the atmosphere, cannot provide a satisfactory fit for all zenith angles. The approximate directional emissivity ϵ_a with the computed coefficients c and m do not provide a good fit when θ is 70° or 80°.

The direct contribution from the surface to the measurement $B(T_m)$ is thus $c \exp(-m/\mu)B(T_s) \exp(-\tau_s/\mu)$, where τ_s is the scattering optical thickness of the layer. The indirect contribution comes from scattering in the τ_s layer illuminated by the flux from the surface. The upward-scattered contribution to the observation $B(T_m)$ measured from space at the zenith resulting from this illumination by the layer is denoted as B_{sc} (where sc stands for scattering cloud). This illumination is assumed to increase with the optical path length τ_s/μ along an inclined direction as $1 - \exp(-\tau_s/\mu)$, and the emerging radiances are assumed to be the same at the top and bottom of the layer. These assumptions are accurate for an optically thin layer when scattering is by molecules and particles that are small relative to the wavelength.[22] Downward-scattered radiance also contributes to the satellite-received signal by reflection from the water, where mirror reflection $1 - \epsilon(\mu) = 1 - c \exp(-m/\mu)$ is assumed, and subsequent penetration through the scattering layer, specified by $\exp(-\tau_s/\mu)$. Thus the satellite-received signal is given

by

$$B(T_m) = c\exp(-m/\mu)B(T_s)\exp(-\tau_s/\mu) + B_{sc}[1 - \exp(-\tau_s/\mu)] \times \{1 + [1 - c\exp(-m/\mu)]\exp(-\tau_s/\mu)\}. \quad (20)$$

Equation (20) will specify $B(T_m)$ for our analysis after B_{sc} is expressed in terms of $B(T_s)$ and τ_s.

The primary illumination by the surface is the intercepted fraction of the surface emission, and thus the spectral flux ϕ_0 scattered from both sides of a layer with optical thickness τ_s is

$$\phi_0 = 2\pi cB(T_s)\int_0^1 \mu\exp(-m/\mu)[1 - \exp(-\tau_s/\mu)]d\mu/\pi = 2cB(T_s)[E_3(m) - E_3(m + \tau_s)], \quad (21)$$

where E_3 is the exponential integral $E_3(x) = \int_0^1 \mu\exp(-x/\mu)d\mu$.

There is an additional illumination of the scattering layer resulting from downward scattering, which is specified by $B_{sc}[1 - \exp(-\tau_s/\mu)]$, a reflection from the water, which is specified by $1 - c\exp(-m/\mu)$, and scattering in the layer of the surface reflection, which is specified by $[1 - \exp(-\tau_s/\mu)]$. Thus the secondary illumination $\Delta\phi$ from the first reflection is

$$\Delta\phi = 2B_{sc} \times \int_0^1 \mu[1 - \exp(-\tau_s/\mu)]^2[1 - c\exp(-m/\mu)]d\mu = B_{sc}\{1 + 2[E_3(2\tau_s) - cE_3(m) - 2E_3(\tau_s) - cE_3(2\tau_s + m) + 2cE_3(\tau_s + m)]\} = B_{sc}(1 + 2\Sigma E_3), \quad (22)$$

where in the last expression ΣE_3 stands for the five exponential functions E_3 above (in braces).

The total emerging flux scattered (both above and below) is denoted by ϕ, i.e., $\phi = \phi_0 + \Delta\phi$. Integrating the radiances $B_{sc}[1 - \exp(-\tau_s/\mu)]$ over the two hemispheres at the top and the bottom of the layer adds up to ϕ. Thus B_{sc} can be evaluated in terms of the flux ϕ:

$$0.5\phi = 0.5(\phi_0 + \Delta\phi) = 2B_{sc}\int_0^1 \mu[1 - \exp(-\tau_s/\mu)]d\mu = B_{sc}[1 - 2E_3(\tau_s)]. \quad (23)$$

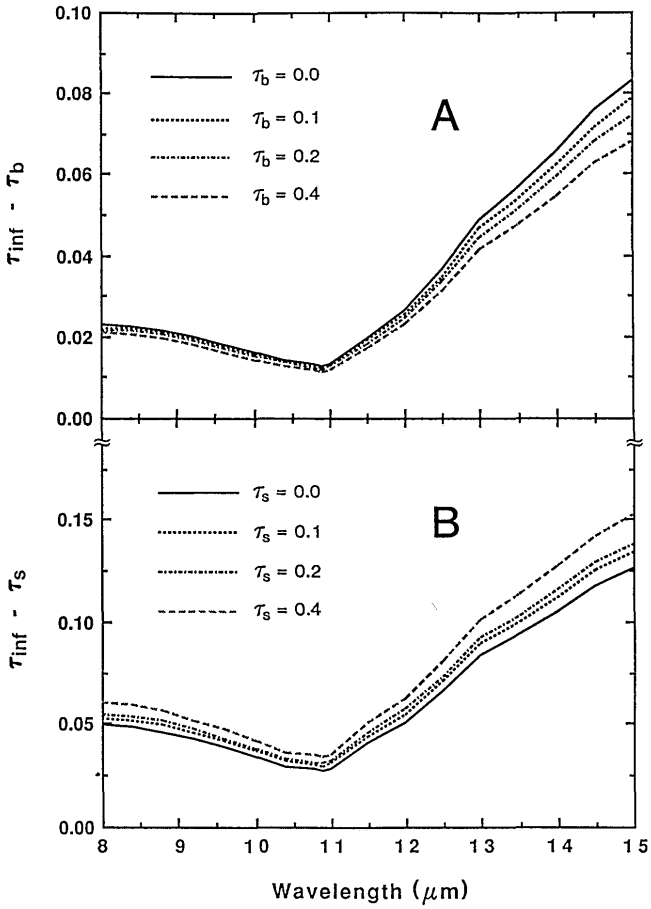

Fig. 7. Error in the inferred optical thickness as in Fig. 6 but with viewing from $\theta = 50°$.

From Eq. (23), expressing ϕ_0 by Eq. (21) and $\Delta\phi$ by Eq. (22), we obtain B_{sc} in terms of $B(T_s)$ and τ_s:

$$B_{sc} = \frac{2cB(T_s)[E_3(m) - E_3(m + \tau_s)}{1 - 4E_3(\tau_s) - 2\Sigma E_3}. \quad (24)$$

With B_{sc} expressed by Eq. (24), Eq. (20) becomes

$$B(T_m) = cB(T_s)\left(\exp[-(m + \tau_s)/\mu] + \frac{2[E_3(m) - E_3(m + \tau_s)][1 - \exp(-\tau_s/\mu)]\{1 + [1 - c\exp(-m/\mu)]\exp(-\tau_s/\mu)\}}{1 - 4E_3(\tau_s) - 2\Sigma E_3}\right). \quad (25)$$

The temperature differences $T_m - T_s$, with $T_s = 300$ K, are plotted for the no-atmosphere case and for three values of τ_s in Fig. 2C for $\theta = 0°$ and in Fig. 3C for $\theta = 50°$. These differences are smaller in magnitude than in the case of emission or absorption by a cirrus cloud, $T_c = 230$ K, plotted in Figs. 2A and 3A, but are much larger than in the case of emission or absorption in the mixed layer, $T_c = 300$ K, plotted in Figs. 3B and 3C. The differences always increase in magnitude with the increasing optical thickness τ_s.

The surface temperature T_{sbb} under the blackbody

assumption is obtained by the inversion of Eq. (25) with $m = 0$ and $c = 1.0$; thus

$$T_{sbb} = B^{-1}\{B(T_m)2[1 + \exp(-\tau_s/\mu)]^{-1}\}. \quad (24)$$

With $B(T_m)$ specified by Eq. (25), the errors $T_{sbb} - T_s$ in the water temperature retrieved under the blackbody assumption are calculated and plotted in Fig. 4C for viewing from the zenith and in Fig. 5C for viewing from $\theta = 50°$. We note that for $\theta = 0°$, Fig. 4C, the underestimate $T_{sbb} - T_s$ slightly increases with increasing optical thickness τ_s, whereas for $\theta = 50°$, Fig. 5C, it slightly decreases.

To understand these rather complicated relationships, we are reminded [see Eqs. (4) and (5)] that the underestimates of the SST under the blackbody assumption stem from two distinct sources: (a) nonemission from the water surface along the direction of the measurement, proportional to $1 - \epsilon(\theta)$, which results in the incorrect assessment of the radiance from the surface at zenith angle θ, part of which is transmitted directly (coefficient of transmission t) to the instrument, and (b) nonemission into the hemisphere, proportional to $1 - \epsilon_h$, which corresponds to the incorrect assessment of the flux emitted by the surface, which is then scattered upward in the direction of the instrument (scattering coefficient $\bar{f}$). Error (b), of course, does not apply in the case of a purely absorbing atmosphere. In measurements from the zenith, error (a) is rather small inasmuch as $\epsilon(0°)$ is close to 1.0. The hemispheric nonemission, the hemispheric reflectance $1 - \epsilon_h$, is significantly higher than the directional nonemission, the reflectance $1 - \epsilon(\theta)$. Thus error (b), which increases with increasing optical thickness, predominates, and the overall underestimate $T_{sbb} - T_s$ increases with increasing optical thickness. However, for measurements at the zenith angle of 50°, error (a) is significant, inasmuch as $\epsilon(50°)$ departs significantly from 1.0, and the overall underestimate $T_{sbb} - T_s$ decreases with increasing optical thickness.

Under the blackbody assumption the scattering optical thickness τ_s is inferred from the measured T_m and the specified T_s, applying the equation

$$\tau_{inf} = -\mu \ln\left[\frac{2B(T_m)}{B(T_s)} - 1\right]. \quad (25)$$

Equation (27) is a restatement of Eq. (26), where T_s replaces T_{sbb}. The errors $\tau_{inf} - \tau_s$ are plotted in Fig. 6B when viewing from the zenith and in Fig. 7B when viewing from $\theta = 50°$, for four values of τ_s in each case. The errors around 11 μm increase only slightly with the optical thickness τ_s. They are smallest, 0.02–0.03 for $\theta = 0$ and 0.03–0.04 for $\theta = 50°$, and largest above 14 μm, up to 0.15.

7. Discussion and Conclusions

The aim of this study was to gain an understanding of how anisotropic emission of a water body affects remotely sensed long-wave data. To examine this problem, we present a formulation of water emission from a calm body for a facile computation of radiative transfer in the atmosphere. With the emissivity specified by the exponential function $c \exp(-m/\mu)$ of the zenith-angle cosine, the radiative transfer computations are expressed in terms of the exponential integral E_3 and thus are relatively simple. The analysis indicates that the blackbody assumption leads to appreciable errors in the retrieved SST and in the inferred optical thickness of a cloud layer.

The underestimates in the inferred SST range from 0.5 (at 11 μm, viewing from the zenith) to 5 K or more. The underestimates are much larger at the viewing zenith angle of 50° than at the zenith and depend on the wavelength of measurement, increasing steeply from the 10- to 12-μm spectral interval to the 12- to 14-μm interval. This theoretical assessment applies in the absence of atmosphere. Actual retrieval errors, whether the instrument is above or within the atmosphere, can be significantly smaller.

The errors in the SST retrieval and in the cirrus cloud characterization stem from the void caused by less-than-unity emission from the surface, i.e., partial nonemission for a given temperature. The reflection from the water of the atmospheric component, whether stemming from atmospheric emission or from backscattering, tends to fill in this void of the nonunity emission. The error reduction depends on the characteristics of the atmosphere: the absorbing versus the scattering properties, the optical thickness, and the temperature of the emission. An absorbing atmosphere always reduces the errors, increasingly so with a larger optical thickness and a higher temperature. The errors in the measurements from space and at any level within the atmosphere are the same. When viewing above it, a scattering layer slightly reduces the errors at large-view zenith angles, but slightly increases them at the zenith. In a retrieval from aircraft data obtained within the scattering layer, the errors are not the same as in measurements from space.

The aim of the near-future satellite programs is to derive the SST with an accuracy of 0.1 K. Our results force the conclusion that the nonunity emissivity of water has to be incorporated in the inversion. Inaccurate assessment of the actual emissivity may cause particularly significant problems at wavelengths above 12 μm, where the departures from the blackbody are strong. The uncertainties in defining atmospheric absorption and scattering coefficients introduce additional errors. These are not analyzed here and are left for a planned future study.

The inference of the optical thickness of an absorbing layer under the blackbody assumption can be in error by $\Delta\tau$ of 0.01 to 0.08 (in the estimated optical thickness). The error $\Delta\tau$ is not a sensitive function of the actual optical thickness or of the view direction, but it does depend steeply on the wavelength of the measurement. Larger errors, by a factor of 2 at least, can be expected in inferring the optical thickness of a scattering layer. Because the index of refraction of water in the 8- to 15-μm interval

changes significantly with the wavelength, it is especially important to address the actual anisotropy of emission when characterizing the size distribution of cloud particles on the basis of the inferred spectral dependence of the optical thickness.

The above analysis was presented as being applicable to a flat surface, i.e., a calm-water body. Water emissivities and reflectances *can* be appreciably different for a stormy sea. The sea state produces a wind-dependent distribution of slopes, as analyzed from Sun glitter by Cox and Munk.[23–25] For a wind speed of 10 m/s, they report an effective slope of 13.1°. The emissivity at a given viewing zenith angle θ to the surface then becomes an effective average of emissivities at zenith angles to a slope normal that are both smaller and larger than θ. For zenith viewing, such averaging involves look directions only at larger zenith angles, i.e., with lower emissivities. The reduction of emissivity to the zenith by this averaging is essentially insignificant, because for a fairly large cone around the perpendicular viewing the emissivities decrease slowly with the zenith angle. At the other extreme, viewing just under the horizon, averaging involves look directions predominantly with larger emissivities (than the emissivity at the zenith angle θ to a horizontal surface).

One must consider surface-emitted and subsequently surface-reflected (from an adjoining slope) photons as another aspect of the sea state. These surface-emitted, surface-reflected (SESR) photons from a structured sea surface contribute to an enhanced effective emissivity. Examining the situation when a slope at the extreme inclination α_c faces a slope also inclined at α_c but with normal in the opposite quadrant, we observe that the SESR photons are all reflected at zenith angles larger than $90° - 3\alpha_c$. The SESR photons therefore do not contribute to the emissivity near the zenith unless α_c approaches 30°.

Based on the points brought up in the previous two paragraphs (that the emissivity decreases slowly departing from perpendicular viewing and that SESR photons are not directed to near the zenith) and on our simplified calculations (presented in Appendix A), assuming that there are no steep slopes in the distribution of wave-slope inclinations, we conclude that emissivities (reflectances) are essentially unchanged by the sea state when viewing near the zenith, as determined by Masuda *et al.*[26] The errors stemming from the blackbody assumption in the SST measurements from the zenith and near zenith under an absorbing atmosphere are therefore the same for a calm sea as well as under sea-state conditions. The underestimates that we evaluate should be compared with the negative bias of 0.3 to 0.4 K in the temperatures derived from satellite measurements versus ship data, found by McClain *et al.*[6] when there is no tuning in the retrieval.

At intermediate zenith angles the sea-state effects on emissivity are somewhat uncertain, inasmuch as the effects can depend on the details of slope distributions. The measurement of sea state from the same satellite, such as that available on European Space Agency ERS 1, is a distinct advantage. With increasing viewing zenith angle θ, the averaging of the emissivities over a cone of inclinations to the slopes (which range from $\theta - \alpha_c$ to $\theta + \alpha_c$) produces an appreciable reduction in the emissivity, as found by Masuda *et al.*[26] and as established by a simplified calculation in Appendix A for $\theta = 50°$. An important point to consider is that sea state produces an even steeper increase in the reflection (reduction in the effective emissivity) when the incident radiation originates from an optically thin absorbing layer. In the case of such a thin layer, the water emissivity at $\theta + \alpha_c$ is weighted much more heavily in computing the effective emissivity than that at $\theta - \alpha_c$. This point suggests that great care must be exercised when choosing the emissivity in radiative transfer calculations. The findings of Saunders[27] that the average infrared-window radiance for oblique viewing increases with roughness is not inconsistent with our results: The measured radiances (in Woods Hole, Mass.) under rough conditions include enhanced contributions of the atmospheric emission (at long paths through near-surface layers). For θ above 50°, the SESR photons can be expected to start contributing significantly to the emissivity. At these intermediate values of θ, there is thus a crossover of the sea-state effect from emissivity reduction to its enhancement. At large zenith angles the directional emissivities are increased steeply by sea state.[17]

Sea-spray effects on the emissivity under stormy conditions may produce some muting of the zenith-angle dependence. Water-vapor continuum emission at near-surface levels, which is quite strong over a wide range of wavelengths,[28] mitigates the effects of nonblackbody water emission. In view of the ambitious programs of multidirectional and multispectral space observations planned for the near future, further studies of these problems are warranted.

Appendix A

Oceans are seldom so calm that the water surface can be regarded as flat, as a horizontal plane. Our calculations based on Bramson's emissivity data can be directly applicable in situations fairly common over lakes, but rather rare over the seas. Under stormy conditions, the water surface has a distribution of slopes. Steeper slopes become more important with increasing wind speed and fetch. For a wind speed of 10 m/s, Cox and Munk[23–25] reported that the effective slope is 13.1°. In the distribution, slopes steeper than that are obviously encountered with decreasing probability. In these situations of slope distributions, directional emissivity from the surface has to be calculated over a distribution of the view zenith angles to the different slopes, all of which contribute to the radiance emitted along the specified direction.

In their analysis of the problem, Masuda *et al.*[26] computed the ocean emissivities viewing from differ-

ent directions, under various sea-state conditions. Their detailed research involved integration over distribution of slopes, as formulated by Cox and Munk.[25] To gain further insight into this complicated problem, we present a simplified, possibly simplistic, scheme for assessing the emission and reflection under sea-state conditions. We apply the scheme to discuss the effective reflection in two advanced infrared scanner (AIRS) spectral bands.

For the water surface under 10 m/s wind with an effective slope (for Sun-glitter reflection) of 13.1°, we assume that only slopes at an inclination of $\alpha = 13.1°$ exist in the distribution. Inasmuch as there are no slopes larger than 13.1°, simple considerations (see Fig. 8A) establish that photons emitted from one slope and reflected by mirror reflection from another slope leave the surface at zenith angles larger than $90° - 3 \cdot 13.1° = 50.7°$. Thus these SESR photons contribute to the directional surface emissivity $\epsilon(\theta)$ only when viewing at zenith angles $\theta > 50.7°$. SESR photons enhance the hemispheric emissivity, but we do not analyze these effects. Our calculations presented below (of reflection from an absorbing atmosphere) will apply only to directions within the vertical cone $\theta \leq 50.7°$.

We consider the geometry involved in the emission or reflection from the sloping waves in Fig. 8. The slopes are represented as planar facets, perpendicular to the plane of this figure. Inasmuch as the emission

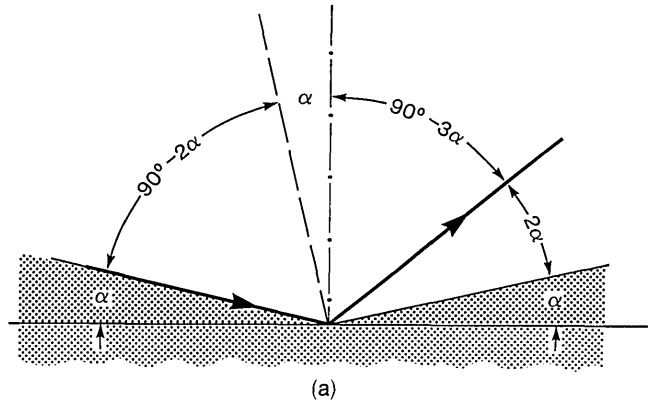

(a)

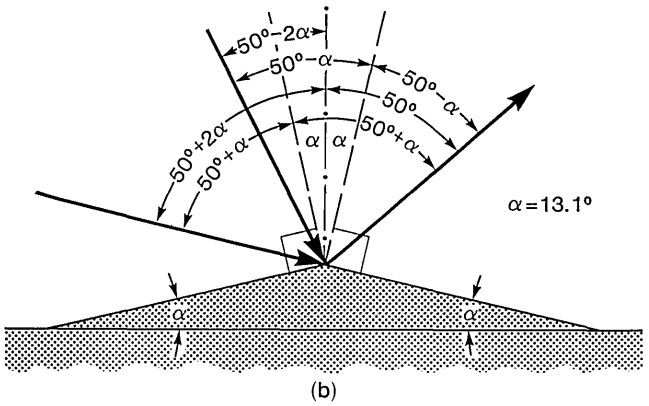

(b)

Fig. 8. Geometry of emission and reflection under sea-state conditions.

at a zenith angle θ accrues at inclinations to a facet of $\theta \pm \alpha$, the emissivity ϵ_1 under sea-state conditions at zenith angle θ is specified as

$$\epsilon_1(50°)B(T_s) = \frac{[\cos(\theta + \alpha)\epsilon(\theta + \alpha) + \cos(\theta - \alpha)\epsilon(\theta - \alpha)]}{\cos(\theta + \alpha) + \cos(\theta - \alpha)} B(T_s). \quad \text{(A1)}$$

The plus applies when the emitted radiance and the facet normal are in the same quadrant. The zenith angle $\theta - \alpha$ applies (instead of the angle $\theta + \alpha$) when the facet normal lies in the quadrant other than the direction of emission as shown in Fig. 8.

For emission to the zenith, the extreme zenith angle to the facet normal equals the inclination of the facet, i.e., 13.1°. Inasmuch as the emissivity decreases only slowly with the zenith angle around the zenith, we can easily conclude that sea state affects the emissivity to the zenith in a negligible way. For emission at a zenith angle of 50°, shown in Fig. 8B on the right, the extreme zenith angles to a facet are 50° ± 13.1°, i.e., 36.9° and 63.1°. Inasmuch as the emissivity begins to drop steeply at a zenith angle of ~50°, the average of the emissivities at 36.9° and 63.1° will be significantly smaller than the emissivity at 50° (which is the only zenith angle to consider under calm conditions). This phenomenon forces us to conclude that sea state does reduce the emissivity in the direction $\theta = 50°$, and that a more detailed examination is warranted.

We evaluate $\epsilon_1(0°)$ and $\epsilon_1(50°)$ for the sea state corresponding to a wind speed of 10 m/s^{-1} in two spectral bands of the AIRS, 10.9 and 13 μm, using in Eq. (A1) a multiterm fit to $\epsilon(\theta)$ as specified by Bramson.[14] The calculated reflectances $1 - \epsilon_1$ are presented in Table 1. We note that $\epsilon_1(0°)$ is essentially the same as $\epsilon(0°)$ (lower by less than 1 part in 10^3). As we discussed, this similarity was to be expected inasmuch as the emissivity $\epsilon(\theta)$ decreases slowly with θ in this region. However, $\epsilon_1(50°)$ is significantly lower than $\epsilon(50°)$. An opposite situation arises at very large zenith angles just under the horizon (85°–90°), when in the averaging, emissivities

Table 1. Directional Reflectances $1 - \epsilon(\theta)$, Directional Reflectances $1 - \epsilon_1(\theta)$, and Conical-To-Directional Reflectances ρ_1 for the Same Sea State as a Function of Optical Thickness of the Atmospheric Layer τ_s[a]

	λ = 10.9 μm		λ = 13.0 μm	
θ	0°	50°	0°	50°
$1 - \epsilon(\theta)$	0.00699	0.01448	0.03030	0.04962
$1 - \epsilon_1(\theta)$	0.00700	0.02075	0.03030	0.05992
$\rho_1(\tau_b = 0.05)$	0.00700	0.03124	0.03030	0.08132
$\rho_1(\tau_b = 0.1)$	0.00700	0.03069	0.03030	0.08020
$\rho_1(\tau_b = 0.2)$	0.00700	0.02962	0.03030	0.07802
$\rho_1(\tau_b = 0.3)$	0.00700	0.02863	0.03030	0.07599

[a]Reflectances $1 - \epsilon(\theta)$ are as tabulated in Ref. 14; reflectances $1 - \epsilon_1(\theta)$ are computed for the sea state corresponding to 10 m/s wind; conical-to-directional reflectances ρ_1 for the same sea state. All reflectances are for viewing zenith angles 0 of 0° or 50°.

higher than that in the view direction are predominantly encountered. Thus a decreased emissivity under the sea state conditions at $\theta = 50°$ that we report, which is in agreement with the more accurate calculations of Masuda *et al.*,[26] is not inconsistent with the increased emissivity for a stormy sea observed and discussed by Ben-Shalom *et al.*[17] At zenith angles larger than 50.7° the SESR photons contribute to an enhanced emissivity ϵ_1. Thus 50° is approximately the limiting (largest) zenith angle for which our simple formulation of ϵ_1, in which the contribution of SESR photons is disregarded, applies.

The above conclusion can be reached solely from reflectance comparisons, whatever the emission downward from the atmosphere is. Isotropic (zenith-angle-independent) emission should not be assumed in our study, inasmuch as we are concerned with measurements in the atmospheric windows, which implies a low optical thickness. In analyzing the reflected radiance it behooves us to examine the products of the down radiance and associated reflectance. For emission with an absorbing optical thickness of, e.g., 0.1, the down radiance will be proportional to $1 - \exp(-0.1/\cos\theta)$. This expression changes from 0.0952 at the zenith to 1.0 at the horizon, i.e., by an order of magnitude. This change means a much heavier weighing of the low emissivity in considering reflection from a cone of impinging radiances.

The directional emissivity $\epsilon_1(\theta)$ that we computed above therefore loses its direct applicability to the assessment of the reflection from the surface. Calculations of the radiance reflected at a zenith angle θ must be formulated considering the distribution of the radiances in the downwelling atmospheric flux. As seen in Fig. 8, values of the radiances within zenith angles $\theta \pm 2\alpha$ are involved in computing the reflected radiance. We have to integrate (in general integrating over a cone of downwelling radiances, but only summing over two zenith angles in our simplified case) the products of an atmospheric radiance and a reflectance from a facet. As we demonstrated in the previous paragraph, in the distributions of these products larger reflectances (at larger zenith angles) will generally multiply higher atmospheric radiances (again, at larger zenith angles). Thus a possible ambiguity exists concerning the meaning of the directional reflectance, whether it is the ratio of the reflected radiance to the downwelling conical flux (of all the incident radiances that contribute to this reflected radiance) or to the downwelling radiance at the center of the cone.

The facet reflection of radiance emitted downward by an absorbing layer characterized by T_c and τ_b is specified as

$$B(T_c)\{1 - \exp[-\tau_b/\cos(\theta + 2\alpha)]\} \times \cos(\theta + \alpha)[1 - \epsilon(\theta + \alpha)],$$

where $\theta - 2\alpha$ and $\theta - \alpha$ should be substituted when the facet normal is in a different quadrant than the reflection direction. This situation, that the radiance reflected to a given direction depends on the distribution of the incoming radiation (i.e., depends on τ_b), has an exact parallel at solar wavelengths (for non-Lambertian surfaces), where the reflected radiance is not specified by the magnitude of global irradiation but depends, e.g., on the ratio of scattered to direct irradiation.

To avoid possible ambiguity, we define the unidirectional radiance (UNR) ratio ρ_1 as the ratio of a reflected radiance to the downwelling radiances from a region (a cone) of the atmosphere. This ratio ρ_1 is given as

$$\rho_1(\theta) = \frac{\sum_{\alpha} \cos(\theta + \alpha)\{1 - \exp[-\tau_b/\cos(\theta + 2\alpha)]\}[1 - \epsilon(\theta + \alpha)]}{\sum_{\alpha} \cos(\theta + \alpha)\{1 - \exp[-\tau_b/\cos(\theta + 2\alpha)]\}}, \quad \text{(A2)}$$

where the summation extends in our simplistic case over only two values of α, $\alpha = 13.1°$ and $\alpha = -13.1°$.

Calculations of ρ_1 thus involve an assumption about the optical thickness τ_b of the downward-emitting layer. The UNR ratios $\rho_1(0°)$ and $\rho_1(50°)$ are computed for the two AIRS bands 10.9 and 13 μm with values of τ_b ranging from 0.05 to 0.3. In these narrow bands the absorption by water-vapor continuum predominates, with absorption at 13 μm by a factor of ~3 higher than that at 10.6 μm.[28] The results are presented in Table 1. From the zenith the sea-state UNR ratio $\rho_1(0°)$ is only insignificantly larger than the calm-water reflectance $1 - \epsilon(0°)$, but the UNR ratio $\rho_1(50°)$ is much larger than $1 - \epsilon(50°)$ and significantly larger than the previously computed (for isotropic emission, i.e., for $\tau_b \gg 1.0$) sea-state reflectance $1 - \epsilon_1(50°)$. We note that the optical thickness τ_b has an appreciable influence on the value of the UNR ratio at $\theta = 50°$, which becomes significantly larger in cases of low optical thickness τ_b, but it has essentially no influence at $\theta = 0°$.

Joseph Otterman and David Kratz acknowledge the support of NASA in this study. Helpful comments by T. W. Brakke, M. -D. Chou, R. S. Fraser, D. Kimes, and C. Prabhakara of NASA/Goddard Space Flight Center and by C. Jusem of GSC, are gratefully appreciated. The manuscript was carefully typed by M. Hall of GSC.

References

1. C. Prabhakara, R. S. Fraser, G. Dalu, M. -L. C. Wu, and R. J. Curran, "Thin cirrus clouds: seasonal distribution over oceans deduced from Nimbus-4 IRIS," J. Appl. Meteorol. **27,** 379–399 (1988).
2. C. Prabhakara, J.-M. Yoo, G. Dalu, and R. S. Fraser, "Deep optically thin cirrus clouds in the polar regions: part I. Infrared extinction characteristics," J. Appl. Meteorol. **29,** 1313–1329 (1990).
3. C. Prabhakara, G. Dalu, and V. G. Kunde, "Estimation of sea surface temperature from remote sensing in the 11 to 13 μm window region," J. Geophys. Res. **79,** 5039–5044 (1974).
4. T. B. Barnett, W. C. Patzert, S. C. Webb, and B. R. Bean, "Climatological usefulness of satellite determined sea surface temperatures in the tropical pacific," Bull. Am. Meteorol. Soc. **60,** 197–205 (1979).
5. J. Susskind, J. Rosenfield, D. Reuter, and M. T. Chahine, "Remote sensing of weather and climate parameters from HIRS2/MSU on TIROS-N," J. Geophys. Res. **89,** 4677–4697 (1984).
6. E. P. McClain, W. G. Pichel, and C. C. Walton, "Comparative performance of AVHRR based multi-channel sea surface temperatures," J. Geophys. Res. **90,** 11587–11601 (1985).
7. J. Susskind and D. Reuter, "Retrieval of sea-surface temperatures from HIRS2/MSU," J. Geophys. Res. **90,** 11602–11608 (1985).
8. A. E. Strong, "Greater global warming revealed by satellite-derived sea surface temperature trends," Nature (London) **338,** 642–645 (1989).
9. R. W. Reynolds, C. K. Folland, and D. E. Parker, "Biases in satellite-derived sea-surface-temperature data," Nature (London) **341,** 728–731 (1989).
10. I. J. Barton, A. M. Zavody, D. M. O'Brien, D. R. Cutten, R. W. Saunders, and D. T. Llewellyn-Jones, "Theoretical algorithms for satellite-derived sea surface temperatures," J. Geophys. Res. **94,** 3365–3375 (1989).
11. A. E. Strong, "Monitoring El Niño using satellite-based sea surface temperatures," Ocean-Air Interact. **1,** 11–28 (1986).
12. E. P. McClain, "Global sea surface temperatures and cloud clearing for aerosol optical depth estimates," Int. J. Remote Sensing **10,** 763–769 (1989).
13. D. Friedman, "Infrared characteristics of ocean water (1.5–15 μm)," Appl. Opt. **8,** 2073–2078 (1969).
14. M. A. Bramson, *Infrared Radiation: A Handbook of Applications* (Plenum, New York, 1968).
15. M. Sidran, "Broad-band reflectance and emissivity of specular and rough water surface," Appl. Opt. **20,** 3176–3183 (1981).
16. G. A. Maul, "Zenith angle effects in multichannel infrared sea surface remote sensing," Remote Sensing Environ. **13,** 439–451 (1983).
17. A. Ben-Shalom, J. Otterman, and P. Schechner, "Measured infrared radiances near sea horizon and their interpretation—preliminary results," Geophys. Res. Lett. **8,** 772–774 (1981).
18. G. Dalu, "Emittance effect on the remotely sensed sea surface temperature," Int. J. Remote Sensing **6,** 733–740 (1975).
19. T. Takashima and Y. Takayama, "Emissivity and reflectance of the model sea surface for a use of AVHRR data of NOAA satellites," Pap. Meteorol. Geophys. **32,** 267–274 (1981).
20. J. Kornfeld and J. Susskind, "On the effects of surface emissivity on temperature retrievals," Mon. Weather Rev. **105,** 1605–1608 (1977).
21. W. L. Wolfe and G. Zissis, *The Infrared Handbook* (U.S. Department of the Navy, Washington, D.C., 1978).
22. J. Otterman, "Single-scattering solution for radiative transfer through a turbid atmosphere," Appl. Opt. **17,** 3431–3438 (1978).
23. C. Cox and W. Munk, "Statistics of the sea surface derived from Sun glitter," J. Mar. Res. **13,** 198–227 (1954).
24. C. Cox and W. Munk, "Measurement of the roughness of the sea surface from photography of the Sun's glitter," J. Opt. Soc. Am. **44,** 835–850 (1954).
25. C. Cox and W. Munk, "Some problems in optical oceanography," J. Mar. Res. **14,** 63–78 (1955).
26. K. Masuda, T. Takashima, and Y. Takayama, "Emissivity of pure and sea waters for the model sea surface in the infrared window regions," Remote Sensing Environ. **24,** 313–329 (1988).
27. P. M. Saunders, "Radiance of sea and sky in the infrared window 800–1200 cm^{-1}" J. Opt. Soc. Am. **58,** 645–652 (1968).
28. D. E. Burch, "Radiative properties of the atmospheric windows," presented at the Conference on Atmospheric Radiation, Fort Collins, Colo., 7–9 August 1972.
29. R. W. Spencer and J. R. Christy, "Precise monitoring of global temperature trends from satellites," Science **247,** 1558–1562 (1990).